Korean J. Chem. Eng., **29**(4), 421-431 (2012)
DOI: 10.1007/s11814-012-0032-1

INVITED REVIEW PAPER

Progress and prospects in thermolytic dehydrogenation of ammonia borane for mobile applications

Junshe Zhang and Jae W. Lee†

Department of Chemical Engineering, The City College of New York, New York, NY 10031, USA
(*Received 4 January 2012 • accepted 8 March 2012*)

Abstract−Using hydrogen as a transportation fuel has been attracting considerable interest due to zero carbon emissions from vehicles. Storing hydrogen compactly, safely and affordably remains a major scientific and technological challenge in on-board applications. Over the past decade, significant efforts have been made in developing solid-state hydrogen storage techniques. Among the chemical storage materials, ammonia borane is one most promising candidate because it has a high hydrogen density of 19.6 wt% and it is a non-flammable and non-explosive crystalline compound at ambient conditions. Hydrogen can be extracted from ammonia borane via thermolysis, hydrolysis, hydrothermolysis, and methanolysis. This review covers various approaches and prospects of facilitating thermolysis, along with a brief discussion of the nature of ammonia borane and the regeneration of spent fuel.

Key words: Hydrogen Storage, Ammonia Borane, Thermolytic Dehydrogenation

INTRODUCTION

Hydrogen is a promising energy carrier. It has a high gravimetric energy density (142 MJ/kg) - at least three times higher than that of other chemical fuels, e.g., the equivalent value for liquid hydrocarbon is 47 MJ/kg - and it has a low environmental impact because water is the only combustion product. It can be produced from various sources like water, biomass, and other organic compounds [1]. Burning H_2 electrochemically in a fuel cell to produce electricity (and heat) that drives an engine has twice higher efficiency than burning petroleum in an internal combustion engine [1]. On the other hand, H_2 has a relatively low volumetric energy density - it is 0.01 kJ/L for gaseous hydrogen at STP and 8.4 MJ/L for liquid hydrogen - compared with that of gasoline (34 MJ/L) [2,3].

For mobile applications, an energy carrier should possess both a small weight to maintain fuel efficiency and a small volume to accommodate more passengers. Recently, the U.S. Department of Energy (DOE) has set new targets for onboard H_2 storage systems for light-duty vehicles travelling longer than 300 miles on a single fill, e.g., the updated 2017 gravimetric density and volumetric density is 5.5 kg H_2/kg and 4.7 MJ/L or 70 Kg/m^3 (based on the whole system which includes not only the storage materials but also valves, tanks, regulators, piping, insulation, etc.), respectively, at delivery temperatures of −40 to 80 °C [4]. And, the vehicles also require safe and affordable containment. Therefore, storing hydrogen compactly, safely and affordably poses a major obstacle to on-board use of hydrogen.

Currently, there are four leading approaches to hydrogen storage: physical means (high-pressure tanks), porous solids (carbon materials, metal-organic frameworks, organic molecular crystals, etc.), metal hydrides (AlH_3, LiH, MgH_2, $LaNi_5H_6$, $Li_3Be_2H_7$, Mg_2NiH_6, $Mn_2ZrH_{3.6}$, $Y_5Fe_{23}H_{20}$, etc.) and complex and chemical hydrides ($NaAlH_4$, $Li_3Na(NH_2)_4$, $NaBH_4$, $Mg(BH_4)_2$, $LiNH_2BH_3$, $N_2H_4(BH_3)_3$, NH_4BH_4, NH_3BH_3, etc.) [1,5-14]. High pressure hydrogen has a gravimetric density of 100 wt% and a volumetric density less than 40 Kg/m^3 (at pressures up to 70 MPa). By contrast, metal hydrides have gravimetric densities below 15 wt% and volumetric densities ranging from 60 to 160 Kg/m^3. The porous solids and complex and chemical hydrides have gravimetric densities between 4 and 25 wt% and volumetric densities ranging from 40 to 170 Kg/m^3 (Fig. 1). Among these materials, ammonia borane (NH_3BH_3, AB) is one of the most attractive candidates, because it has a gravimetric hydrogen density of 19.6 wt% and a volumetric hydrogen density of around 145 Kg/m^3 and it is a non-flammable and non-explosive white solid at normal temperature and pressure conditions [12,14]. Hydrogen release from AB can be achieved through several options, including thermolysis (i.e., thermal decomposition or pyrolysis) [14-17], hydrolysis [14,18,19], combined hydrolysis and thermolysis (hydrothermolysis) [20-22], and methanolysis [14,23-25]. Hydrothermolysis is a promising option to liberate around 9 wt% hydrogen at a tem-

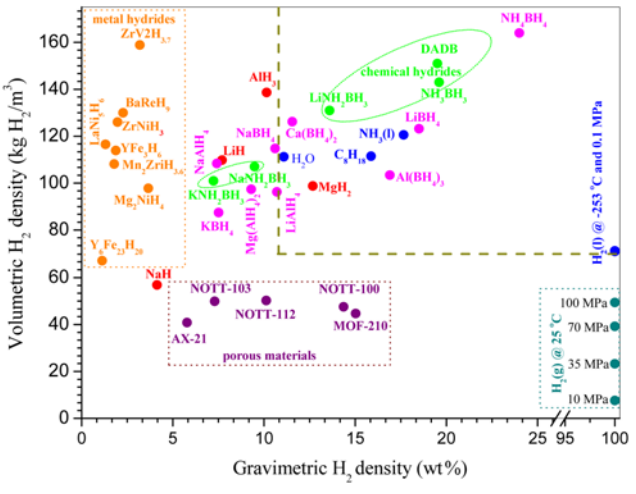

Fig. 1. Gravimetric H_2 density (wt%) plotted against volumetric H_2 density (kg H_2/m^3) for selected representative potential hydrogen storage materials (Modified from ref 12).

†To whom correspondence should be addressed.
E-mail: lee@che.ccny.cuny.edu

perature lower than 90 °C. However, since thermolysis alone has a potential for generating more than 9 wt% hydrogen at the same temperature range, this review will focus on recent efforts in the thermal decomposition of AB. Neither hydrolysis nor methanolysis is covered in this review because hydrogen storage capacity is lowered due to the amount of water and methanol. First, we will present the properties of AB, followed by a brief discussion of methods of synthesizing AB. Then, we will describe the thermolysis of AB in detail. The next section will deal with various approaches to promote AB thermolysis at relatively low temperatures for PEM fuel cell operation, followed by a section on recycling the spent AB, and then we provide a brief conclusion.

PROPERTIES OF AB

Ammonia borane is isoelectronic with gaseous ethane, but it contains a highly polarized dative N→B bond that is formed through the electron donor-acceptor pair. And, the dissociation energy of N→B bond (ca. 130 kJ/mol) is much stronger than a typical van der Waals interaction [26]. In addition, nitrogen-bonded hydrogen (positively charged or protic H) and boron-bonded hydrogen (negatively charged or hydridic H) atoms can form dihydrogen bonds (N-H···H-B) in the solid phase, which has been confirmed by spectroscopic studies [27-30]. As a result, ammonia borane is a stable molecular crystalline compound under ambient conditions. This molecular crystal transfers from a disordered tetragonal structure (I4mm, a=b=0.5240 nm and c=0.5028 nm) to an ordered orthorhombic structure ($Pmn2_1$, a=0.5517 nm, b=0.4742 nm and c=0.5020 nm) with a transition enthalpy of 1.34 kJ/mol, as it is cooled from room temperature to −48 °C at atmospheric pressure [30,31]. It was found that the transition is triggered by the NH_3 rotor motion based on the ^{15}N NMR measurements. ^{15}N NMR investigations suggested the transition is also of displacive type [32]. On the other hand, Raman spectroscopic studies revealed that there are three solid-to-solid phase transitions, occurring at approximately 2, 5 and 12 GPa, respectively, as the crystalline solid was pressurized to 22.3 GPa at room temperature [29]. However, there is no agreement on the number of phase transitions and the pressure at which the phase transition occurs in terms of Raman spectroscopic observations [28-30]. The detailed crystal structure of AB under extremely high pressures, however, remains not well characterized.

For the thermal decomposition of AB for mobile applications, the thermal properties of AB are of great interest from the viewpoint of designing hydrogen storage systems. However, there are a few reports on the thermochemical and thermophysical properties. The thermal conductivity of AB is about 15 W/m·°C at room temperature, and it increases linearly to around 36 W/m·°C at 147 °C [33]. These data were obtained by using ASTM E1225 method. One problem associated with the thermal conductivity at high temperatures is that AB melts and/or decomposes under these conditions; thus, the values at high temperature are less reliable compared with that at ambient temperature. At 25 °C, the heat capacity, molar standard entropy and molar enthalpy difference of AB is 75.4 J/mol·°C, 96.3 J/mol·°C and 15.2 kJ/mol, respectively [31]. According to the variation of thermodynamic properties with temperature at a range of −48 to 25 °C, it is expected that the heat capacity increases as the temperature becomes high. Unfortunately, the data at high temperatures is not available in literature. Also, the enthalpy of AB melting has not been determined because of the overlap of the thermal decomposition of AB with the phase transition under normal conditions, which makes it impossible to identify the endpoint of melting.

SYNTHESIS OF AB

To realize AB as a commercially viable hydrogen storage material, synthesizing AB efficiently and economically is being pursued. Ammonia borane can be synthesized via either metathesis of ammonium salts and MBH_4 (where M is Na or Li) or displacement of borane complexes with ammonia [23,34,35]. The former method has been well studied, whereas the later one is less investigated. Table 1 presents a detailed comparison of two routes for AB synthesis, and it shows that PNNL route gives both high yield and purity compared with the Purdue one. Furthermore, it was expected that PNNL route can produce AB on a commercial scale at ca. US $9/kg if the price of $NaBH_4$ is as low as US $5/kg [35]. It should be noted here that the cost of AB is referred to the fresh fill.

THERMAL DECOMPOSITION OF AB IN SOLID STATE

The thermolysis behavior of AB has been widely studied since

Table 1. A comparison of two routes for AB synthesis (modified from ref. 35)

	PNNL	Purdue
B source	$NaBH_4$	$NaBH_4$
N source	NH_4Cl	NH_4HCO_2
Solvent	THF and NH_3	Dioxane
Yield	99%	95%
Purity	99%	98%
Reaction conditions	−70 °C, 0.1 MPa or 25 °C, 2 MPa	40 °C, 0.1 MPa
Feed stoichiometry	Near-stoichiometric	50% excess NH_4HCO_2
Solvent requirements	>2 mol/L $NaBH_4$ in solvent	1 mol/L $NaBH_4$ in solvent
Solvent separation	Distillation	No separation is required
By-product recovery	Separation via solubility difference	Separation of Na and NH_4 slats requires more complex processing
Waste generation	Minimal waste	Moderate liquid waste

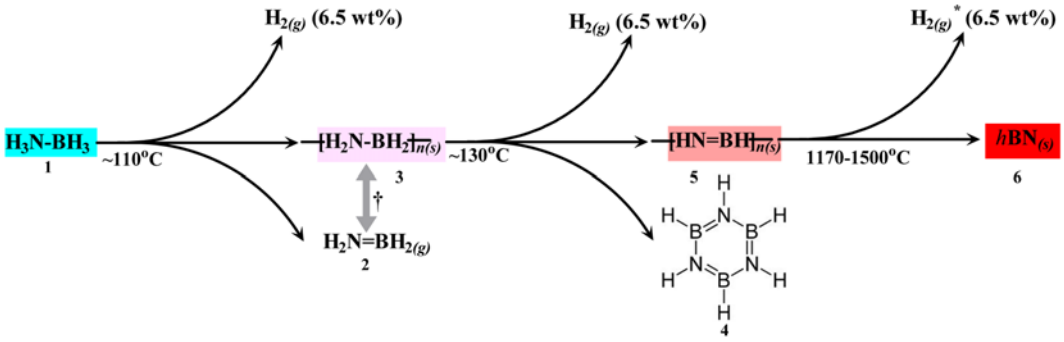

Scheme 1. Experimentally observed pathways for the thermal decomposition of AB (modified from ref. 36). Species involved in ammonia borane pyrolysis: 1, Ammonia Borane; 2, Molecular Aminoborane; 3, Polyaminoborane (PAB); 4, Borazine; 5, Polyiminoborane (PIB); 6, Semi-Crystalline P63/mmc (hexagonal) boron nitride. †, Reversibility between molecular aminoborane and PAB is inferred. *, Hydrogen abstraction by the evolution of molecular hydrogen at high temperature, is assumed, but other possible pathways exist.

it was first investigated by thermogravimetric analysis (TGA) in 1978 [15]. Ammonia borane decomposes in three distinct steps, commencing at ca. 110, 130 and 1,170 °C [36], respectively, with about 6.5 wt% of hydrogen (with respect to the initial mass of AB) liberated in each steps (Scheme 1). Many studies have shown that decomposition behaviors, such as the decomposition temperature and the mass weight loss, are affected by the thermal history to which AB is subjected [15,17,36,37]. It has been found that the onset temperature for the first decomposition step is strongly dependent on the as heating rate, e.g., the first decomposition step commences at ca. 82 and 107 °C at a heating rate of 0.05 and 1 °C/min [37], respectively. The dependence of this onset temperature on heating rate could be interpreted as some active species - compounds that can promote the decomposition - form before the start of decomposition, which is supported by the evidence from the effect of treating AB at low temperatures on the thermolysis behaviors at a temperature range of 50 to 200 °C. Lee and co-workers found that the thermal-treating shifts the first decomposition step to low temperatures but it has insignificant effect on the second decomposition step [38]. Additionally, the melting point of AB is highly variable with the heating rate. At a very low heating rate, e.g., 0.05 °C/min, the solid-liquid phase transition was absent at temperatures up to ca. 116 °C [37], although the thermal decomposition was detected. It was expected that a solid solution most likely exists before the start of melting, because other species could form during heating. More evidence to support the occurrence of other compounds was provided by calorimetric studies. At a heating rate of 1 °C/min, a small but detectable exothermic event preceding the melting was observed [38], which is accompanied by the formation of volatile products. One issue that arises from these observations is whether AB is stable at an extreme temperature (between 60 and 50 °C) for hydrogen storage materials in a fuel cell. Thermal stability analysis shows that AB is stable for ~5.5 day and ~72 day at 60 and 50 °C [39], respectively. Furthermore, the weight loss regarding the solid phase is significantly contingent on the heating rate [17]. At a heating rate of 1 °C/min, the weight loss is around 8 and 15 wt% at in the first and the second decomposition step, respectively. But, at a heating rate of 5 °C/min, it increases to 10 and 23 wt%, respectively. And in extreme cases, it can reach as high as 25 and 50 wt% in the first and the second decomposition step [33]. However, Baitalow and co-workers observed that the yield of hydrogen is independent of the heating rate [17]. Therefore, the variation of weight loss with heating rate exists because the formation of other volatile products including aminoborane ($H_2N=BH_2$), diborane (B_2H_6), ammonia (NH_3) and borazine ($B_3N_3H_6$) is thermal-dependent. The solid products are polyaminoborane (PAB, $NH=NH]_n$), polyiminoborane (PIB, $[NH=NH]_n$), and hexagonal boron nitride (hBN) for the first, second and third decomposition steps [36]. In contrast to the volatile species, the effect of thermal history on the solid product has been less studied. This issue could be very important, because the solid product property is related to the efficiency of regenerating spent fuels. Besides the thermal history, other operating conditions like pressure and atmosphere also have influence on the decomposition.

A differential thermal analysis (DTA) study showed that the weight loss in 7 hr at 90 °C increases from ca. 7 to 24 wt% as the argon pressure decreases from 0.104 to 0.014 MPa [40]. Also, the DTA data revealed that the period elapsed before the onset of weight loss becomes shorter as the pressure decreases, which is attributed to the more crystal defects resulting from AB sublimation as the pressure is lowered. Analyzing the volatile products by mass spectroscopy (MS) further showed that the occurrence of $H_2N=BH_2$, B_2H_6 and $B_3N_3H_6$ becomes important at low pressures [40]. On the other hand, only two distinct decomposition steps were detected by using Raman spectroscopy at 5.5 GPa, occurring at 192-200 and 230-237 °C, respectively [42]. The solid product of the first decomposition step is PAB, where the solid product of the second decomposition is a precursor of hBN, based on Raman spectroscopic and powder X-ray diffraction investigations. Moreover, molecular dynamic (MD) simulations show hydrogen is released via an intermolecular reaction of one AB molecule at ambient pressure but an intermolecular pathway involves three AB molecules at extreme high pressures [42]. From these results, it could be argued that the decomposition shifts to high temperatures with increased pressures.

The thermal decomposition of AB was usually investigated under inert gases like argon (Ar) and helium (He). TGA results, however, show that that the presence of atmospheric gases has a dramatic effect on the decomposition. Suib and co-workers found that heating AB at temperatures up to 400 °C in an Ar atmosphere gives rise to a weight loss as high as 50 wt%, if the instrument is exposed to air, but less than 20 wt% for the case of the instrument being housed in

an Ar filled glovebox [36]. It was proposed that some species like water (H_2O) or oxygen (O_2) could interact with surface sites, resulting in a high yield of other volatile species besides hydrogen. Although there are no studies on the interaction of AB with water vapor or oxygen, decomposing AB in other reactive media implies that either H_2O or O_2 itself or the product of H_2O or O_2 reacting with AB changes the pathway of thermal decomposition. Suib and co-workers also observed that the second decomposition step is endothermic based on differential scanning calorimetric (DSC) investigations without housing the equipment in a glovebox, which is inconsistent with the early reports [36]. An endothermic event associated with the second decomposition step is also reported by Zhang and co-workers [43]. These studies mean that the presence of impurities, either in solid phase or gas phase, and even the method of preparation could markedly influence the second decomposition step. In terms of utilizing AB as an on-board storage material, the effect of trace levels of contaminants on the thermal decomposition is required to be investigated in detail.

The first detailed mechanism for the thermal decomposition in solid state was obtained from the *in-situ* solid state ^{11}B magic angle spinning-nuclear magnetic resonance (MAS-NMR) studies [44]. At temperatures below the melting point, the decomposition is composed of three steps: induction, nucleation, and growth (Scheme 2). In the induction period, a mobile phase of AB (AB^*) results from the disruption of the dihydrogen bond network. Further analyses suggest that AB is crystalline but the environment of N and B in AB^* is more like an isolated molecule than a molecular crystal [45]. Subsequently, new species including diamoniate of diborane (DADB), linear dimer of aminoborane (LDAB), and cyclic dimer of aminoborane (CDAB) appear. Finally, DADB reacts with AB to liberate hydrogen and to produce dimeric, oligomeric, and eventually various polymeric species including linear, branched, and cyclic ones at the same time. For further insight into the role of DADB, the thermal decomposition of DADB-doped AB was studied and the induction period - the time elapsed before hydrogen release is detected after bringing the sample to a desired temperature - is reduced dramatically in the presence of 5 wt% of DADB [46]. Additionally, a comparison between DADB and ammonium chloride (NH_4Cl) effects

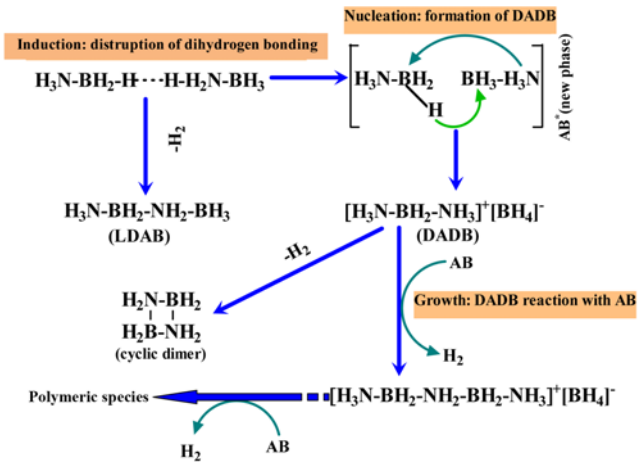

Scheme 2. Proposed mechanism for the thermal decomposition of AB showing discrete induction, nucleation and growth steps leading to hydrogen release (Modified from ref 44).

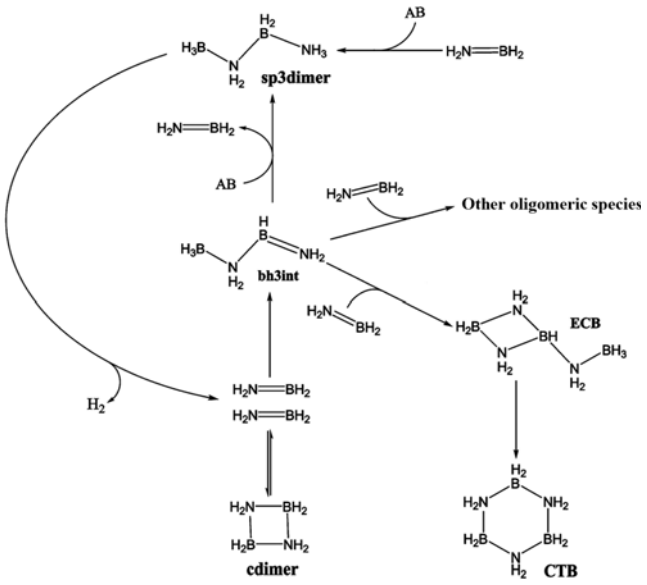

Scheme 3. Possible pathways for the reaction of aminoborane ($H_2N=BH_2$) with ammonia borane or itself, resulting in oligomers in an autocatalytic decomposition. Reprinted from ref. 47. Copyright 2009 American Chemical Society.

on the thermal decomposition suggests the short induction period comes from $[(NH_3)_2BH_2]^+$, the cation of DADB, which is the solid product of ammonium chloride reaction with AB at elevated temperature [46]. Ab initio calculations, however, suggest that DADB dehydrogenation generates aminoborane that reacts with AB to form LDAB. Then one LDAB decomposes into two aminoborane and one dihydrogen. Also, aminoborane could form oligomeric species like cyclic dimers [47]. From these calculations, it was proposed that the generation of additional aminoborane from AB and aminoborane composes an autocatalytic cycle for the thermal decomposition (Scheme 3).

ACCELERATED THERMAL DECOMPOSITION

Although AB has a gravimetric hydrogen density of 19.6 wt% and a volumetric hydrogen density of around 145 Kg/m^3, only two-thirds of hydrogen content is useful because the solid product (hBN) of the third decomposition step is too stable to be regenerated. A significant effort has been made to control the first two decomposition steps, with respect to rapid hydrogen desorption at temperature around 85 °C, the working temperature of polymer electrolyte membrane fuel cell, and avoidance of other volatile products including ammonia and borazine, which can damage a fuel cell. A basic concept behind the acceleration of hydrogen release is to disperse AB in various media such as solid matrix, liquids with or without catalyst, and reactive gases.

1. AB Confined within Mesopores

The first solid medium employed to facilitate the thermal decomposition is SBA-15 [48], one type of mesoporous silica with a 2D hexagonal cylindrical pore structure (its pore diameter is 7.5 nm). It was demonstrated that at a loading level (the mass ratio of AB to mesoporous silica) of 1, the half time, at which the reaction is 50%

is complete, is 85 min at 50 °C for the SBA-15-AB nanocomposite, but it is 290 min at 85 °C for the pristine AB based on isothermal DSC measurements. Additionally, it was found that the formation of borazine was strongly inhibited for nano-confined AB as revealed by temperature programmed desorption (TPD) coupled with MS and solid-state ^{11}B NMR investigations. Furthermore, it was reported that the enthalpy of first decomposition for nano-encapsulated AB was significantly reduced to −1 kJ/mol (−22 kJ/mol for bulk AB [16]). From these observations, it was believed that the formation of other boron-contained species like borazine besides PAB contributes to the greater exothermicity for bulk AB thermolysis. However, the enthalpy of AB decomposition into only hydrogen and PAB has not been measured. Therefore, it remains unclear whether the equilibrium between AB and PAB+H_2 is the same for nano-confined AB as for the bulk AB.

A detailed report on the decomposition of mesoporous silica-AB nanocomposites focused on the effect of loading levels [43]. For MCM-41-AB nanocomposites, the decomposition temperature was found to shift to lower values with decreasing loading levels, and only one decomposition step with a peak temperature around 90 °C was detected at temperatures less than 200 °C in TG-DSC investigations for the loading levels of 0.11 and 0.15 at a hearing rate of 1 °C/min in nitrogen (Fig. 2). Furthermore, hydrogen release measurements showed that 12.6 wt% of hydrogen regarding the mass of AB is liberated from the 0.15 nanocomposite (the number is referred to as the loading level) in 1 hour at 89.5 °C, corresponding to desorption of two equivalents of hydrogen. Interestingly, the release of two equivalents of hydrogen at temperatures below 100 °C was also observed for AB encapsulated in the pores of carbon cryogel (CC) and metal organic framework (MOF) [49,50]. It was deduced that, at sufficient low loading levels, the thickness of nano-encapsulated AB is sub-nanometer, which may require less energy for the thermal decomposition. However, additional mechanistic steps might be involved, for example, the reaction between AB or thermolysis products like PAB and Si-OH groups on the silica surface, which may produce hydrogen during the thermolysis. By using *in-situ* solid state ^{11}B NMR and Fourier transform infrared (FTIR) spectroscopy; it was found that AB nanoconfined in CC could react with hydroxyl groups of CC surface at room temperature [51], resulting in formation of B-O bonds and release of hydrogen. Also, this reaction and/or hydroxyl groups most likely catalyze the thermal decomposition. A subsequent study found that the reaction of AB with hydroxyl groups of mesoporous carbon produces ammonia [52], which is harmful to the fuel cell. The formation of ammonia, however, can be strongly inhibited by lithium (Li)-doping without a negative effect on the decomposition kinetics. Although there is little doubt about the reaction of AB with -OH for the nanocomposites, its influence on the enthalpy of the first decomposition remains elusive [50,52].

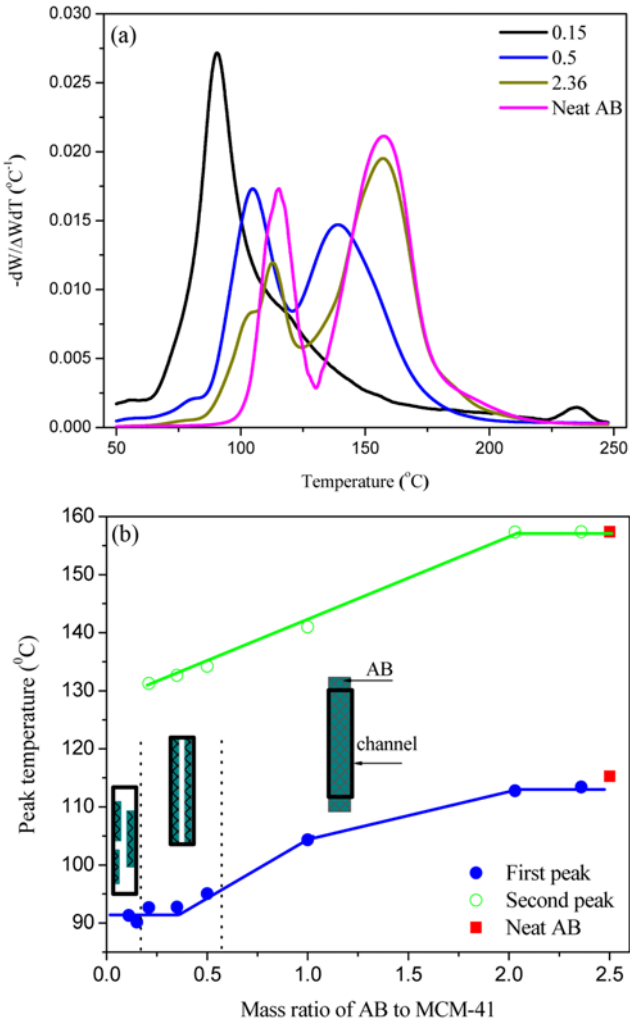

Fig. 2. (a) Relative weight loss rate of neat AB and nanocomposites with different loading levels. ΔW is the mass difference between 50 and 247 °C. (b) Variation of peak temperatures with loading levels. Reprinted from ref 43. Copyright 2011 American Chemical Society.

To obtain more insight into the thermal decomposition behavior of nanocomposites, the nature of these materials was investigated by using hyperpolarized ^{129}Xe NMR, synchrotron X-ray powder diffraction, anelastic spectroscopy, DSC, and X-ray diffraction (XRD) [53-55]. It is evident from ^{129}Xe NMR spectrum that all AB resides inside the pores at loading levels below 0.5, but some AB accumulates outside the pores at loading levels above 0.5 for MCM-41-AB nanocomposites [53]. Synchrotron X-ray powder diffraction data show that the orthorhombic-tetragonal phase transition at −48 °C is absent for the 0.5 MCM-41-AB nanocomposite, and the occurrence of order-disorder phase transition is observed at −48 °C for 1 and 3 MCM-41-AB nanocomposites [54]. Additional evidence for the crystalline state of AB in nanocomposites was obtained from anelastic spectroscopy and DSC investigations [55]. It was observed that no phase transition is detected on Young modulus and DSC curves for the 0.5 MCM-41-AB nanocomposite. XRD analysis also reveals that tetragonal AB is absent at low loading levels, but it appears at high loading levels (above 1) for MCM-41-AB nanocomposites [43]. From these observations, it could be surmised that the nano-confined AB is amorphous.

Another approach to the confinement of AB in a solid matrix is demonstrated by the decomposition behaviors of poly(methyl acrylate)-AB composites [56]. Only one decomposition step with a peak temperature about 95 °C is observed for the 0.2 composite, but two decomposition steps with a sharp peak centered around 96 °C and a weak broad peak ranged from 120 to 150 °C for the 0.8 composite

on the TPD-MS curves at a temperature range of 60 to 220 °C. XRD analyses and DSC studies reveal that tetragonal AB is absent for the former composite but it appears for the latter one. And the existence of tetragonal AB gives rise to the second decomposition step for the 0.8 composite. Interestingly, the formation of borazine was found to be inhibited for these two composites at a heating rate of 2 °C/min. Mechanistically, it was proposed that the low decomposition temperature and the borazine inhibition stem from the interaction between carbonyl groups and AB, resulting in the formation of B-O bonds and occurrence of ammonia. Surprisingly, B-H bonds were not detected in the solid product if the decomposition temperature was ramped up to 220 °C. This means that the reaction of AB with carbonyl groups instead of the decomposition is the dominant reaction at elevated temperatures, which converts all B-H bonds to B-O bonds.

2. AB Dispersed in Liquids

The first open report on promoting the decomposition in liquids using catalysts was provided by Maners and co-workers in 2001 [57]. In the presence of 0.6 mol% of $[Rh(1,5\text{-co})(\mu\text{-Cl})]_2$, it was found that two equivalents of hydrogen is released from AB dissolved in diglyme or tetraglyme in 72 h at 45 °C, and borazine and insoluble oligomeric and/or polymeric B-N species are the other predominant products [57]. In 2006, an exceptional active catalyst was reported by Goldberg and Heinekey [58]. They demonstrated that, with 0.5 mol% of ridium pincer complex, (POCOP)Ir(H)2 (POCOP= η^3-1,3-$(OP^tBu_2)_2C_6H_3$), one equivalent of hydrogen is liberated from AB dissolved in tetrahydrofuran (0.5 mol/L) in 14 min at room temperature, and a white insoluble precipitate is produced. Solid state ^{11}B NMR, XDR and IR investigations suggest that the precipitate is cyclopentaborazane ($[H_2N\text{-}BH_2]_5$). However, the formation of other oligomeric and/or polymeric species cannot be excluded. Subsequently, extremely active ruthenium catalysts were found in 2008 [59]. Fagnou and co-workers reported that, with 0.03 mol% KO^{t}Bu activated Ru catalyst, one equivalent of hydrogen is generated from AB dissolved in THF (5 mol/L) and insoluble polymeric aminoborane species is obtained in 5 min at 20 °C. Schneider and co-workers tested ruthenium complexes with cooperative PNP ($=HN[CH_2CH_2P^iPr_2]_2$) ligands for AB decomposition in THF (0.54 mol/*l*) at room temperature [60]. They observed that, at a catalyst loading of 0.1 mol%, slightly more than one equivalent of hydrogen is evolved in 10 min and a small amount of borazine and polymeric aminoborane species is produced.

Although precious-metal-based catalysts have high activity towards the thermal decomposition in liquids, the prohibitive cost of precious metals makes them less economically viable. The non-precious-metal catalysts are also of considerable interest. Baker and co-workers found that hydrogen desorbs immediately at 60 °C after mixing the solution resulted from $Ni(cod)_2$ reacting with 2 equivalent of N-heterocyclic carbene (NHC) ligands in C_6D_6 with a slurry of 10 equivalent AB in C_6D_6 or a solution in diglyme (bis(2-methoxyethyl)ether) [61]. Further investigations show that, with 10 mol% Ni-NHC catalyst, 2.8 equivalent of hydrogen is produced within 4 h at 60 °C, based on hydrogen release measurements. Very importantly, the yield of borazine is not significant because it is rapidly consumed by subsequent cross-linking reaction. Another type of non-precious-metal catalyst is acid. It was observed that, with 0.5 mol% tris(pentafluorophenyl) borane ($B(C_6F_5)_3$, Lewis acid), 1.1 equivalents of hydrogen is liberated from AB dissolved in tetraglyme (2.6 mol/L) in 20 h at 60 °C [62]. Similar behaviors were also reported for Brønsted acids such as trifluoromethanesulfonic ($HOSO_2CF_3$) acid or even HCl. A subsequent study suggests that the activity of $B(C_6F_5)_3$ could be improved by introducing P^tBu_3, which forms a frustrated Lewis pair with $B(C_6F_5)_3$ in C_6D_5Cl [63].

Homogeneous catalysts could be problematic for regeneration of spent fuels because of complicated separation associated with recovering thermolysis products and catalysts. To avoid this problem, Burrell and co-worker investigated the activity of supported precious metal catalysts [64]. With 2.0 mol% of Pt/Aluminia (0.5%), around 1.5 equivalents hydrogen is produced from AB dissolved in 2-dimethoxyethyl (0.33 mol/L) in 30 min at 70 °C. The catalytic activity, however, decreases over reaction cycles because of insoluble products depositing on the active sites. The deactivated catalyst can be regenerated by either heating it at temperatures above 150 °C for 2-4 h or sonicating it.

Another entirely different approach to enhance the decomposition is to disperse AB in ionic liquids (ILs). Compared with organic solvents, ILs have advantageous properties, including negligible vapor pressure, ability to dissolve various compounds, stability at elevated temperatures, polarity that can stabilize ionic transition states and intermediates, and little loss of activity over cycles [65,66]. Sneddon and co-workers observed that, for the AB and 1-butyl-3-methylimidazolium chloride (bmimCl) solution (mass fraction of AB is 0.5), hydrogen evolves immediately upon placing the mixture in a heated oil bath. Hydrogen release measurements showed that 0.95 equivalent of hydrogen (the amount of hydrogen liberated was measured by using a Toepler pump) is produced in 3 h at 85 °C. By contrast, the hydrogen release from pristine AB is negligible in 3 h at 85 °C. Very interestingly, only traces of borazine were detected for this system [67]. A subsequent report reveals that, for the same system mentioned above, 1.1 and 2.2 equivalents of hydrogen (the amount of hydrogen liberated was determined by using an automated gas buret) are generated in 67 min and 330 min at 85 °C, respectively [68]. From solid and solution ^{11}B NMR studies, it was inferred that ILs induces the formation of DADB, a more reactive species with respect to hydrogen desorption. Additional investigations found that the decomposition in ILs could be further improved by introducing catalysts like base and transition metals [69,70]. It was reported that, with 5.3 mol% non-nucleophilic based bis(dimethylamino)naphthalene (Proton Sponge, PS), 2 equivalents of hydrogen is released in 171 min at 85 °C from AB-bimimCl solutions (50/50 wt%). Also, the results show that PS can catalyze the decomposition of AB either in solid state or in tetraglyme solutions. Solid state and solution ^{11}B NMR investigation suggest that, for PS-promoted reaction, the decomposition starts with the formation of $H_3BNH_2^-$ anion that initiates AB dehydropolymerization to form branched-chain polymeric species and ultimately a cross-linked polyborazylene-like product [69]. In another report, it was shown that, with 5 mol% Ru and Rh-based catalysts ($[Ru(COD)Cl]_2$ and $[Rh(COD)Cl)_2$), around 1.3 equivalents of hydrogen are generated in 6 h at 65 °C from AB-bimimCl solutions (50/50 wt%) [70].

The drawbacks related to dispersing AB in condensed media are: 1) The hydrogen storage capacity is relatively low because the medium does not liberate hydrogen, e.g., the highest material-based storage capacity reported in literature for AB-mesoporous silica nano-

composites and AB-bimimCl solutions is less than 7.5 wt%. 2) The recovery of spent AB for regeneration as well as the recycle of media for multiple uses is of practical concern. 3) The cost of media and catalysts is less economically viable. Thus, the pursuit of effective, light, easily-separable and cheap media continues. Among the other alternatives, gaseous media could meet these criteria.

3. AB Exposed to Gases

The first report by Lee and co-workers in 2011 focused on the promoted effect of carbon dioxide (CO_2), an abundant and naturally occurring material [71]. The thermal decomposition in CO_2 atmosphere was investigated by using a high-pressure DSC, which allows the pressure and heat flow into/out of a closed cell to be monitored simultaneously. It was shown that CO_2 can enhance the decomposition and this promoted effect becomes more pronounced at high CO_2 pressures at 85 °C. On DSC curves, one exothermic event was detected under 0.33 MPa of air, but two exothermic peaks are observed under 0.17 and 0.26 MPa of CO_2 in 1 h at 85 °C. However, only one intense exothermic peak with an unresolved shoulder was evidenced under 0.37 MPa of CO_2 (Fig. 3). Interestingly, as the CO_2 pressure increases from 0.17 to 0.37 MPa, the onset of second exothermic peak occurred earlier and the area of first exothermic peak became large. The first exothermic event was due to the reaction of CO_2 with AB, or intermediates like DADB, or primary decomposition products including LDAB, because the exothermic heat is strongly CO_2 pressure dependent. And hydrogen release measurements show that, under 0.4 MPa of CO_2, 1.3 equivalents of hydrogen is produced in 1 h at 85 °C.

To obtain more insight into the promoted effect, the decomposition products were analyzed by using FTIR, Raman and solid state ^{11}B and ^{13}C NMR (Fig. 4 and 5). IR investigations revealed that the solid product displays the structural features of PAB and it contains C- and O-contained species (C-O, B-O and C=O stretching modes at 1,240, 1,336 and 1,640 cm^{-1}, respectively, appear on the spectrum), indicating that CO_2 is chemically involved in the decomposition. Additional studies found that, at elevated CO_2 pressures, e.g., 2.2 MPa, bands attributable to BH_3 group vanish and IR frequencies associated with C-H stretching mode appear. Further evidence for the CO_2 chemical participation was obtained from NMR spectroscopy. In the ^{11}B solid state MAS-NMR spectrum, a sharp peak at 1.7 ppm and a broad peak at 15.7 ppm are observed, corresponding to tetrahedral BO_4 groups and trigonal BO_3 groups, respectively.

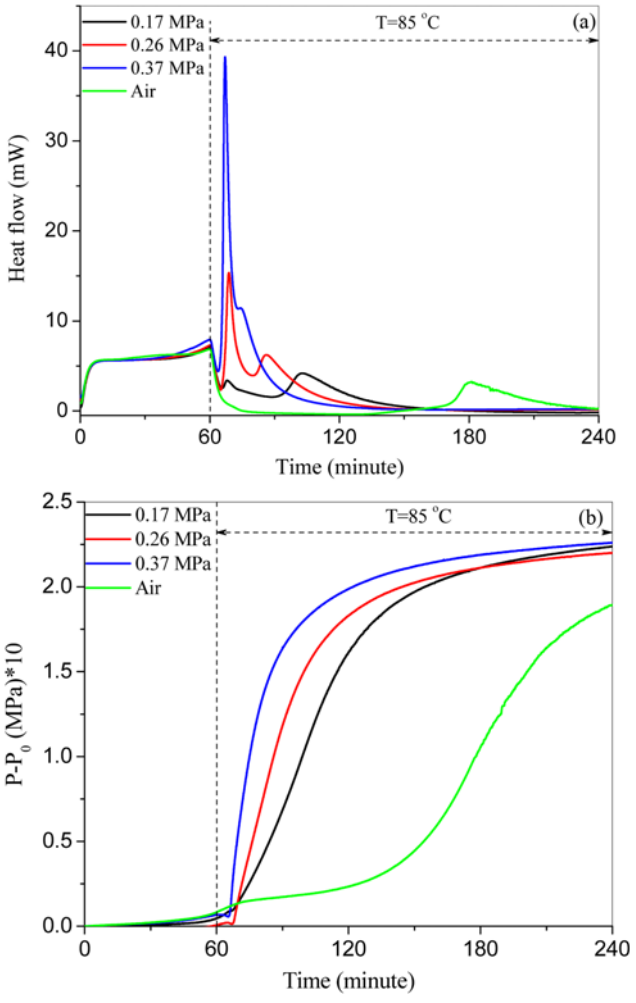

Fig. 3. Heat flow (a) and pressure (b) profiles for AB decomposition with 0.17, 0.26 and 0.37 MPa of CO_2 and 0.33 MPa of air. Reprinted from ref 71. Copyright 2011 American Chemical Society.

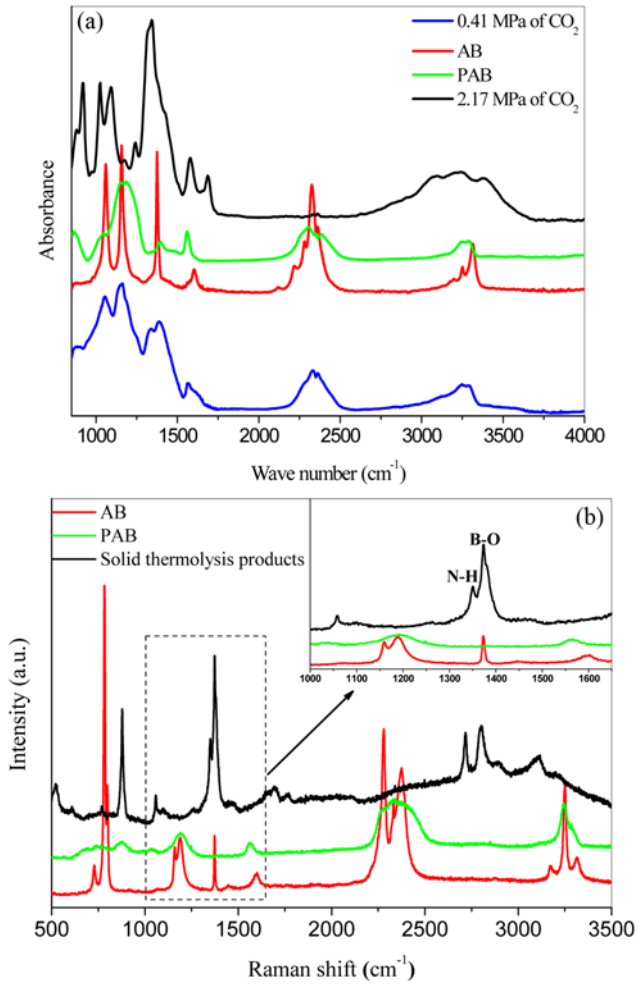

Fig. 4. IR (a) and Raman (b) spectra of AB, PAB and solid decomposition products. Reprinted from ref 71. Copyright 2011 American Chemical Society.

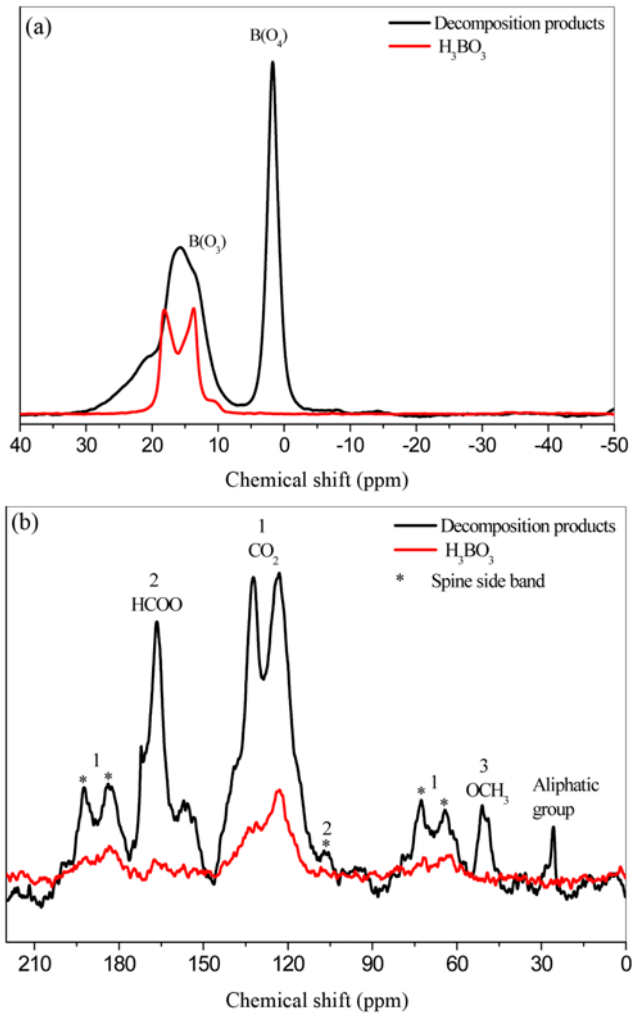

Fig. 5. Solid-state ^{11}B (a) and ^{13}C (b) MAS-NMR of solid decomposition products for 2.17 MPa (at 85 °C) of CO_2. Reprinted from ref 71. Copyright 2011 American Chemical Society.

And the ^{13}C solid MAS-NMR spectrum displays three principal peaks at 25.5, 50.9, and 166.5 ppm besides CO_2 resonances, which are assigned to aliphatic, OCH_3, and HCOO groups, respectively. Upon combining macroscopic findings and microscopic results, it was concluded that CO_2 reacts with AB, or intermediates, or primary decomposition products at 85 °C, which either enhances the concentration of other active species like boronium cations ($[NH_3BH_2NH_3]^+$) or produces catalytic compounds for the decomposition. Based on Raman investigations, it was suggested that CO_2 chemically adsorbs on the crystal surface of AB at ambient temperature, disrupting the hydrogen-bonding network of AB and thus promoting the decomposition. An intermediate species, O---C---O, was also inferred in these investigations. Also, it was proposed that methoxy groups evolve via O=C=O→-O-C=O→-OCH_3 [71]. Nevertheless, the details of the formation of methoxy, formate and aliphatic groups and the role of the reaction of CO_2 with AB in accelerating the decomposition remain unclear at the time of preparing this review.

One issue arising from the introduction of gaseous media is the contamination of hydrogen, which requires the further separation of hydrogen from the other gases. To avoid this problem, Lee and co-workers studied the possibility of treating AB first in CO_2 environments at low temperatures and then performing the decomposition of the treated AB at the target temperature after isolating it [72]. The results revealed that CO_2-treated AB, obtained by keeping pristine AB at 70 °C under 1.38 MPa of CO_2 for 38 min, desorbs 1.5 equivalents of hydrogen in 1 h at 85 °C, corresponding to 10.1 wt% of hydrogen regarding pristine AB. The material-based storage capacity is about 9 wt% after taking into account the mass increase (9-15%), resulting from CO_2 chemical involvement. IR analyses of the solid decomposition product reveal that π-bonded N (e.g., $=NH_2$ groups or segments of $H(HN=BH)_nH$) and B=N bond appear [72]. It was concluded that the high hydrogen yield stems from the large temperature increase at the operating condition, which facilitates more hydrogen desorption. Compared with other promoted options such as using catalysts or dispersing AB in either solid or liquid media, CO_2-induced hydrogen desorption is an eco-friendly and economical approach because only gaseous CO_2 is involved.

REGENERATION OF SPENT AB

Although many efforts have been made to accelerate the decomposition of ammonia borane, there are only a few studies on the regeneration of H_2-depleted AB, which is vital for achieving the full potential of AB as a viable H_2 storage material. The first concept for an energy-efficient regeneration was developed by Mertens and co-workers [73]. The decomposition product (BNH_x) was digested with HCl/$AlCl_3$ in toluene, resulting in the generation of BCl_3 and NH_4Cl (step 1 in Scheme 4). For an energy-efficient recycling process, the formation of diborane (B_2H_6) from BCl_3 is the most challenging step. BCl_3 can be directly reduced to B_2H_6 with H_2 at elevated temperatures (600-750 °C) or metal hydrides at lower temperatures. This procedure, however, is highly energy-consuming or introduces another problem of generating hydrides. It was pointed out that the hydrodechlorination of a $BCl_3 \cdot NR_3$ with H_2 in the presence of an auxiliary base could be carried out at moderate temperatures (step 2 in Scheme 4). One product of this reaction is $BH_3 \cdot NR_3$, which reacts with BCl_3 to produce B_2H_6 (step 4 in Scheme 4). The whole recycling procedure, however, has not been evaluated by experi-

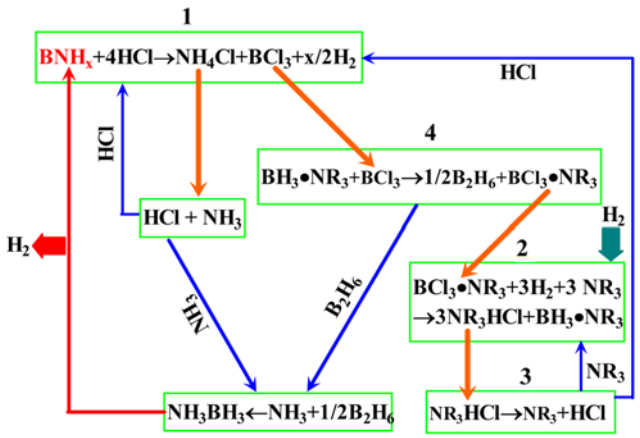

Scheme 4. Strategy for off-board regeneration of ammonia borane from BNH waste (modified from ref. 73).

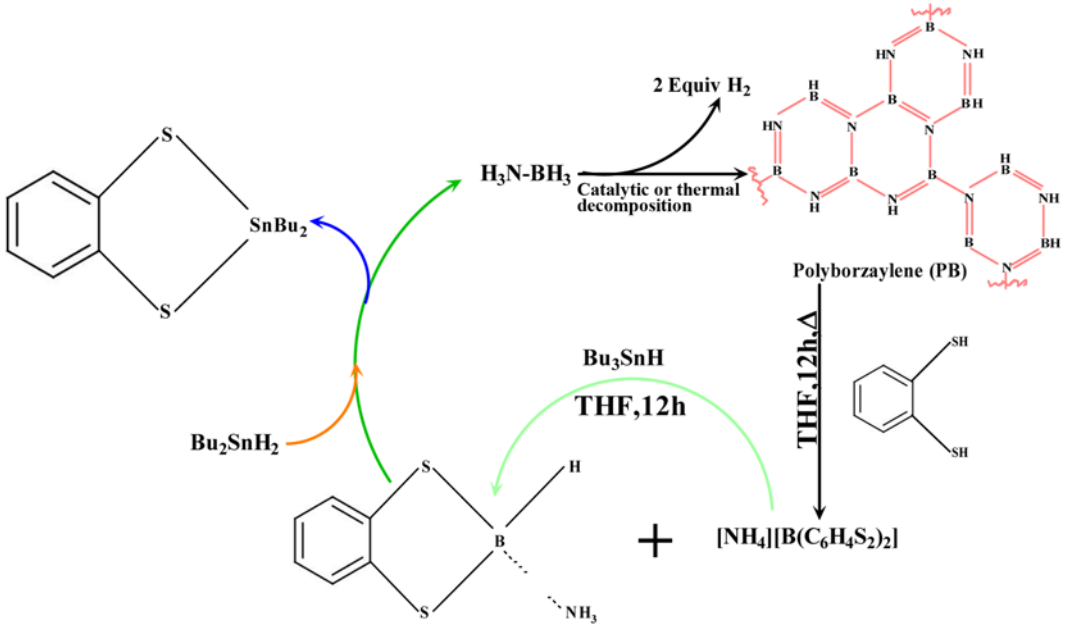

Scheme 5. Possible off-board regeneration pathway for spent ammonia borane (modified from rerf.74).

mental results to confirm its feasibility.

Another regeneration cycle was put forward based on DFT calculation coupled with experimental data or estimates [74]. To avoid the formation of B-O bonds, which are really stable and pose an obstacle for the regeneration, the spent fuel (polyborazylene, PB) was digested with *ortho*-benzenedithiol ($C_6H_6S_2$) in THF, producing $(C_6H_4S_2)$B-H•(NH_3) and $[NH_4][B(C_6H_4S_2)_2]$. The latter can be transformed to the former by using Bu_3SnH as a reductant and with C_6H_4SH(S-$SnBu_3$) as a by-product, converting spent fuel into a single species in two steps. The former compound already has an NH_3 moiety, and thus the thermal cracking to release and recycle NH_3 is not required [Scheme 5]. Subsequently, $(C_6H_4S_2)$B-H·(NH_3) can be reduced to AB by using slight excess of Bu_2SnH_2 (Scheme 5) or with Bu_3SnH via an amine exchange step with Me_3N (Scheme 6). Further investigations showed that dissolving C_6H_4SH(S-$SnBu_3$) in HCl-Et_2O solution yields Bu_3SnCl and $C_6H_6S_2$ in 1 : 1 ratio, and then the isolated Bu_3SnCl can be converted to $Bu_3SnOC(O)H$ via reacting with formic acid in the presence of either NaOH or Et_3N, followed by producing Bu_3SnH from distillation of $Bu_3SnOC(O)H$ at 112 °C under reduced pressure (0.03 MPa) [75].

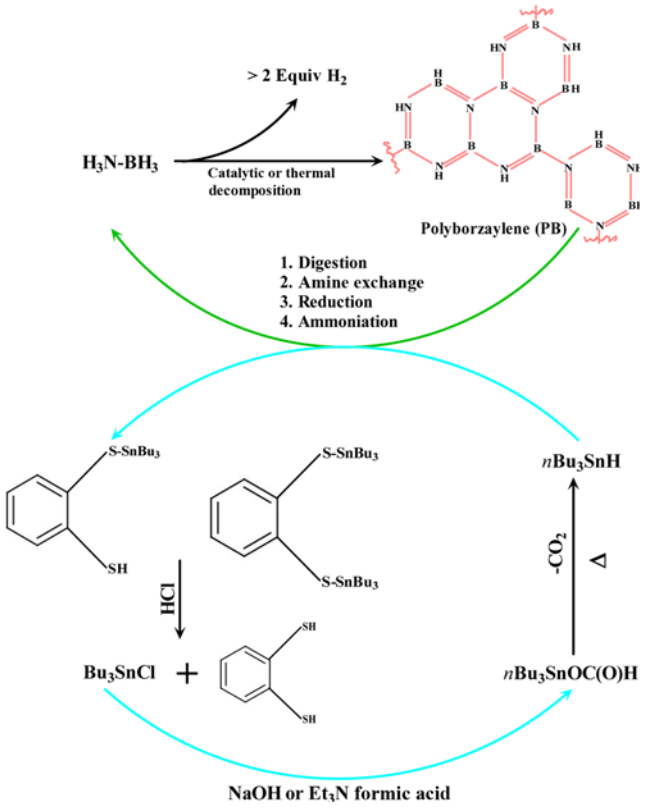

Scheme 6. Off-board regeneration pathway for spent ammonia borane with tin recycle and *ortho*-benzenedithiol recovery (modified from ref. 75).

Very recently, a more energy-efficient and simplified process for AB recycle was proposed by Gordon and co-workers [76]. It has been demonstrated that PB, a material corresponds to a spent fuel derived from the more than 2 equivalents of hydrogen release but it still has some energetic B-H bonds, can be converted back to AB with nitrogen (N_2) as a by-product via treating it with hydrazine (N_2H_4) in liquid ammonia (NH_3) at 40 °C in a sealed pressure reactor. Under the above condition, the yield of AB in 24 h can reach 92%. N_2 can be rehydrogenated to NH_3 and subsequently converted back to N_2H_4. This process not only minimizes the amount of N_2H_4 required to regenerate AB, but also reduces production and recycle costs.

CONCLUSIONS AND PERSPECTIVES

Despite intensive research on ammonia borane over the past decade, its full potential as viable on-board hydrogen storage material has not yet been achieved. For practical applications, around 2.2 equivalents of hydrogen could be extracted from AB because more

hydrogen release results in a hydrogen-depleted material that is too stable to be recyled back to AB, corresponding to 14.3 wt% of hydrogen (regarding the mass of AB). Among numerous approaches of facilitating hydrogen release at 85 °C, the thermal decomposition produces around 10 wt% (with respect to the total mass of AB and other dispersed media) with trace amount of by-products like borazine and ammonia. After taking into account the weight of tanks, valves, regulators, piping, insulation and other equipment, which is around one half of the whole system, no options can meet the current DOE 2017 system target of 5.5 wt%. One promising avenue could be combining CO_2-treatment and metal catalysts, given the highest hydrogen yield for the former and the trace amount of borazine for the latter. To explore this option, the mechanism of CO_2- and metal-catalyzed decomposition is required to be well understood, especially for the CO_2-catalyzed hydrogen release due to few reports on this strategy.

In contrast to the thermal decomposition, the regeneration of spent fuel has been less explored. Although the off-board recycle of polyborazylene back to AB has been demonstrated, it remains unknown whether the real spent fuel can be regenerated via the same route because it contains other species like residual catalyts besides B-N compounds. A further active area could be the effect of decompostion conditions on the reversibility of H_2-depleted AB. And, evetually, the straightfoward and on-board regeneration will be pursued.

REFERENCES

1. L. Schalpbch and A. Züttel, *Nature*, **414**, 353 (2001).
2. C. W. Hamilton, R. T. Baker, A. Staubitz and I. Manner, *Chem. Soc. Rev.*, **38**, 279 (2009).
3. N. C. Smythe and J. C. Gordon, *Eur. J. Inorg. Chem.*, **41**, 509 (2011).
4. http://www1.eere.energy.gov/hydrogenandfuelcells/storage/pdfs/targets_onboard_hydro_storage.pdf.
5. A. C. Dillon, K. M. Jones, T. A. Bekkehdahl, C. H. Klang, D. S. Bethune and M. J. Heben, *Nature*, **386**, 377 (1997).
6. A. C. Dillon and M. J. Heben, *Appl. Phys. A*, **72**, 133 (2001).
7. N. L. Rosi, J. Eckert, M. Eddaoudi, D. T. Vodak, J. Kim, M. O'Keeffe and O. M. Yaghi, *Science*, **300**, 1127 (2003).
8. W. Grochala and P. P. Edwards, *Chem. Rev.*, **104**, 1283 (2004).
9. J. L. C. Rowsell and O. M. Yaghi, *Angew. Chem. Int. Ed.*, **44**, 4670 (2005).
10. A. Karkamkar, S. M. Kathmann, G. K. Schenter, D. J. Heldebrant, N. Hess, M. Gutowski and T. Autrey, *Chem. Mater.*, **21**, 4356 (2009).
11. T. Hügle, M. F. Kühnel and D. Lentz, *J. Am. Chem. Soc.*, **131**, 7444 (2009).
12. W. I. F. David, *Faraday Discuss.*, **151**, 399 (2011).
13. P. Jena, *J. Phy. Chem. Lett.*, **2**, 206 (2011).
14. A. Staubitz, A. P. M. Robertson and I. Manners, *Chem. Rev.*, **110**, 4079 (2010).
15. M. G. Hu, A. Geanangel and W. W. Wendlandt, *Thermochim. Acta*, **23**, 249 (1978).
16. G. Wolf, J. Baumann, F. Baitalow and P. Hoffman, *Thermochim. Acta*, **343**, 19 (2000).
17. F. Baitalow, J. Baumann, G. Wolf, K. Jaenicke-Rößler and G. Leitner, *Thermochim. Acta*, **391**, 159 (2002).
18. M. Chandra and Q. Xu, *J. Power Soruces*, **156**, 190 (2006).
19. Q. Xu and M. Chandra, *J. Power Soruces*, **163**, 364 (2006).
20. M. Diwan, H. T. Hwang, A. Al-Kukhun and A. Varmar, *AIChE J.*, **57**, 259 (2010).
21. H. T. Hwang, A. Al-Kukhun and A. Varmar, *Ind. Eng. Chem. Res.*, **49**, 10994 (2010).
22. J. Zhang, Y. Zhao, D. L. Akins and J. W. Lee, *Ind. Eng. Chem. Res.*, **50**, 10407 (2011).
23. P. V. Ramachandran and P. D. Gagare, *Inorg. Chem.*, **46**, 7810 (2007).
24. S. B. Kalidindi, U. Sanyal and B. R. Jagirdar, *Phys. Chem. Chem. Phys.*, **10**, 5870 (2008).
25. S. Caliskan, M. Zahmakiran and S. Ozkar, *Appl. Catal. B*, **93**, 397 (2010).
26. A. Haaland, *Angew. Chem. Int. Ed. Engl.*, **28**, 992 (1989).
27. S. Trudel and D. F. R. Gilson, *Inorg. Chem.*, **42**, 2814 (2003).
28. R. Custelcean and Z. A. Dreger, *J. Phys. Chem. B*, **107**, 9231 (2003).
29. Y. Lin, W. L. Mao, V. Drozd, J. Chen and L. Daemen, *J. Chem. Phys.*, **129**, 234509 (2008).
30. S. Xie, Y. Song and Z. Liu, *Can. J. Chem.*, **87**, 1235 (2009).
31. G. Wolf, J. C. van Miltenburg and U. Wolf. *Thermochim. Acta*, **317**, 111 (1998).
32. O. Gunaydin-Sen, R. Achey, N. S. Dalal, A. Stowe and T. Autrey, *J. Phys. Chem. B*, **111**, 677 (2007).
33. N. Mohajeri, A. T-Raissi and K. K. Ramasamy, *Thermochim. Acta*, **452**, 28 (2007).
34. D. J. Heldebrant, A. J. Karkamkar, J. C. Linehan and T. Autrey, *Energy Environ. Sci.*, **1**, 156 (2008).
35. http://www.hydrogen.energy.gov/pdfs/review10/st042_linehan_2010_o_web.pdf.
36. S. Frueh, R. Kellett, C. Mallery, T. Molter, W. S. Willis, C. King'ondu and S. L. Suib, *Inorg. Chem.*, **50**, 783 (2011).
37. G. Wolf, J. Baumann, F. Baitalow and P. Hoffman, *Thermochim. Acta*, **343**, 19 (2000).
38. J. S. Zhang, Y. Zhao, D. L. Akins and J. W. Lee, *J. Phys. Chem. C*, **114**, 19529 (2010).
39. S. D. Rassat, C. L. Aardahl, T. Autrey and R. S. Smith, *Energy Fuels*, **24**, 2596 (2010).
40. O. Palumbo, A. Paolone, P. Rispoli, R. Cantelli and T. Autrey, *J. Power Soruces*, **195**, 1615 (2010).
41. J. Nylén, T. Sato, E. Soignard, J. L. Yarger, E. Stoyanov and U. Häussermann, *J. Chem. Phys.*, **131**, 104506 (2009).
42. Y. Liang and J. S. Tse, *J. Phys. Chem. C*, **116**, 2146 (2012).
43. Y. Zhao, J. S. Zhang, D. L. Akins and J. W. Lee, *Ind. Eng. Chem. Res.*, **50**, 10024 (2011).
44. A. C. Stowe, W. J. Shaw, J. C. Linehan, B. Schmid and T. Autrey, *Phys. Chem. Chem. Phys.*, **9**, 1831 (2007).
45. W. J. Shaw, M. Bowden, A. Karkamkar, C. J. Howard, D. J. Heldebrant, N. J. Hess, J. C. Linehan and T. Autrey, *Energy Environ. Sci.*, **3**, 796 (2010).
46. D. J. Heldebrant, A. Karkamkar, N. J. Hess, M. Bowden, S. Rassat, F. Zheng, K. Rappe and T. Autrey, *Chem. Mater.*, **20**, 5332 (2008).
47. P. M. Zimmerman, A. Paul, Z. Zhang and C. B. Musgrave, *Inorg. Chem.*, **48**, 1069 (2009).
48. A. Gutowska, L. Li, Y. Shin, C. M. Wang, X. S. Li, J. C. Linehan, R. S. Smith, B. D. Kay, B. Schmid, W. Shaw, M. Gutowski and T. Autrey, *Angew. Chem. Int. Ed.*, **44**, 3578 (2005).
49. A. Feaver, S. Sepehri, P. Shamberger, A. Stowe, T. Autrey and G. Z. Cao, *J. Phys. Chem. B*, **111**, 7469 (2007).

50. Z. Li, G. Zhu, G. Li, S. Qiu and X. Yao, *J. Am. Chem. Soc.*, **132**, 1490 (2010).
51. S. Sepehri, A. Feaver, W. J. Shaw, C. J. Howard, Q. Zhang, T. Autrey and G. Z. Cao, *J. Phys. Chem. B*, **111**, 14285 (2007).
52. L. Li, X. Yao, C. Sun, A. Du, L. Cheng, Z. Zhu, C. Yu, J. Zou, S. C. Smith, P. Wang, H.-M. Cheng, R. L. Frost and G. Q. Lu, *Adv. Funct. Mater.*, **19**, 265 (2009).
53. L.-Q. Wang, A. Karkamkar, T. Autrey and G. J. Exarhos, *J. Phys. Chem. C*, **113**, 6485 (2009).
54. H. Kim, A. Karkamkar, T. Autrey, P. Chupas and T. Proffen, *J. Am. Chem. Soc.*, **131**, 13749 (2009).
55. A. Paolone, O. Palumbo, P. Rispoli, R. Cantelli, T. Autrey and A. Karkamkar, *J. Phys. Chem. C*, **113**, 10321 (2009).
56. J. Zhao, J. Shi, X. Zhang, F. Cheng, J. Liang, Z. Tao and J. Chen, *Adv. Mater.*, **22**, 394 (2010).
57. C. A. Jaska, K. Temple, A. J. Lough and I. Manners, *Chem. Commun.*, 962 (2001).
58. M. C. Denney, V. Pons, T. J. Hebden, D. M. Heinekey and K. I. Goldbergy, *J. Am. Chem. Soc.*, **128**, 12048 (2006).
59. N. Blaquiere, S. Diallo-Garcia, S. I. Gorelsky, D. A. Black and K. Fagnou, *J. Am. Chem. Soc.*, **130**, 14034 (2008).
60. M. Käss, A. Friedrich, M. Drees and S. Schneider, *Angew. Chem. Int. Ed.*, **48**, 905 (2009).
61. R. J. Keaton, J. M. Blacquiere and R. T. Baker, *J. Am. Chem. Soc.*, **129**, 1844 (2007).
62. F. H. Stephens, R. T. Baker, M. H. Matus, D. J. Grant and D. V. Dixon, *Angew. Chem. Int. Ed.*, **46**, 746 (2007).
63. A. J. M. Miller and J. E. Bercaw, *Chem. Commun.*, **46,** 1709 (2010).
64. R. P. Shrestha, H. V. K. Diyabalanage, T. A. Semelsberger, K. C. Ott and A. K. Burrell, *Int. J. Hydrog. Energy*, **34**, 2616 (2009).
65. T. Welton, *Chem. Rev.*, **99**, 2071 (1999).
66. J. Dupont, R. F. de Suoza and P. A. Suarez, *Chem. Rev.*, **102**, 2667 (2002).
67. M. E. Bluhm, M. G. Bradley, R. Butterick III, U. Kusari and L. G. Sneddon, *J. Am. Chem. Soc.*, **128**, 7748 (2006).
68. D. W. Himmelberger, L. R. Alden, M. E. Bluhm and L. G. Sneddon, *Inorg. Chem.*, **48**, 9883 (2009).
69. D. W. Himmelberger, C. W. Yoon, M. E. Bluhm, P. J. Carroll and L. G. Sneddon, *J. Am. Chem. Soc.*, **131**, 14101 (2009).
70. W. R. H. Wright, E. R. Berkeley, L. R. Alden, R. T. Baker and L. G. Sneddon, *Chem. Commun.*, **47**, 3177 (2011).
71. J. S. Zhang, Y. Zhao, D. L. Akins and J. W. Lee, *J. Phys. Chem. C*, **115**, 8386 (2011).
72. R. Xiong, J. S. Zhang, Y. Zhao, D. L. Akins and J. W. Lee, *Int. J. Hydrog. Energy*, **373**, 3344 (2012).
73. S. Hausdorf, F. Baitalow, G. Wolf and O. R. L. Mertens, *Int. J. Hydrog. Energy*, **33**, 608 (2008).
74. B. L. Davis, D. A. Dixon, E. B. Garner, J. C. Gordon, M. H. Matus, B. Scott and F. H. Stephens, *Angew. Chem.*, **121**, 6944 (2009).
75. A. D. Sutton, B. L. Davis, K. X. Bhattacharyya, B. D. Ellis, J. C. Gordon and P. P. Power, *Chem. Commun.*, **46,** 148 (2010).
76. A. D. Sutton, A. K. Burrell, D. A. Dixon, E. B. Garner III, J. C. Gordon, T. Nakagawa, K. C. Ott, J. P. Robinson and M. Vasiliu, *Science*, **331**, 1426 (2011).

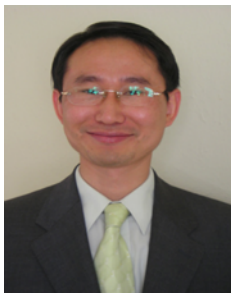

Jae W. Lee is currently a Professor in the Chemical Engineering Department of the City College of New York (CCNY), USA. He obtained his B.S. and M.S. from Seoul National University and received Ph.D. in Designing Reactive Separation Systems from Carnegie Mellon University in 2000. From 2000 to 2001, he was an Alexander Humboldt Research Fellow in Aachen Technical University in Germany. He joined the City College of New York in 2001. His area of research interests includes CO_2 capture and conversion, H_2 storage, energy conversion, natural gas storage/recovery in hydrates, prevention of hydrates for flow assurance, ab initio modeling of hydrate systems, and green engineering via reactive separation. He has delivered numerous invited/keynote lectures in academia and professional societies.